International Journal of Microwave and Wireless Technologies

cambridge.org/mrf

Highly selective, fractal-configured UWB-FSS for sub-6 GHz 5G, GSM, WLAN, and C band electromagnetic stealth application

Chandranath Chattopadhyay[1], Srimita Coomar[2], Santanu Mondal[2] and Rajarshi Sanyal[3]

[1]Institute of Electronics and Telecommunication Engineers, Kolkata, India; [2]Institute of Radio Physics & Electronics, University of Calcutta, Kolkata, India and [3]ECE Department, MCKV Institute of Engineering, Howrah, India

Research Paper

Cite this article: Chattopadhyay C, Coomar S, Mondal S, Sanyal R (2023). Highly selective, fractal-configured UWB-FSS for sub-6 GHz 5G, GSM, WLAN, and C band electromagnetic stealth application. *International Journal of Microwave and Wireless Technologies* **15**, 1731–1744. https://doi.org/10.1017/S1759078723000442

Received: 17 May 2022
Revised: 28 March 2023
Accepted: 29 March 2023

Keywords:
Frequency-selective surface; Minkowski island; selectivity factor; ultra-wideband

Corresponding author:
Chandranath Chattopadhyay;
E-mail: cchandranath22@gmail.com

Abstract

A miniaturized and flexible frequency-selective surface (FSS) has been presented in this article with a unit cell size of $0.049\,\lambda c \times 0.049\,\lambda c$ where λc is the free space wavelength at the lower cut-off frequency. In order to achieve an ultra-wide (−3 dB) second order pass band of 151.3% with enhanced selectivity factor of 0.887, a cascaded triple layered hybrid resonating structure has been proposed with symmetrical Minkowski island-shaped fractal geometry pair and spiral-shaped middle layer in optimized air gap coupling. Furthermore, 149.8% ultra-wide pass band also ascertains the conformal feature of the proposed structure. In addition to this, the proposed FSS provides the stable angular response for both TE and TM polarization. An equivalent circuit model has been synthesized for accurate frequency response. Finally, a sample prototype has been fabricated to verify the experimental validation. Excellent angular stability under large oblique incident and significant conformal characteristics ensure the compatibility of the proposed structure for electromagnetic stealth in 0.9–1.8 GHz GSM band, 2.10–2.14 GHz wireless medical telemetry band, 2.4–2.5 and 4.9–5.8 GHz WLAN band, 3.4–3.7 and 4.4–4.9 GHz sub-6 GHz 5 G band, and 3.7–4.2 GHz C band.

Introduction

Frequency-selective surface (FSS) is traditionally created from the periodic arrangement of two-dimensional metallic patch or aperture on the dielectric substrate. The patch type resonant array element exclusively exhibits the stop band for electromagnetic (EM) waves whereas the pass band response can be achieved by the aperture type FSS. Recently, the role of FSS is drawing immense attention among the researchers mainly due to its wide pass band feature. Single-layered structure always suffers due to limited bandwidth of pass band characteristics. However, intuitively selecting the proper cascading arrangement, the wide flat pass band response with stable performance may be achieved [1]. In this regard, numerous approaches have been proposed throughout the decades. A simple mechanism of pass band enhancement is the cascading of capacitive and inductive metallic layer [2–4]. Multiple ring slots and split-ring slots loading on square unit cell develop the wider pass band in [5]. The second-order pass band with fast roll-off has also been discussed in [6]. A total number of in band transmission pole improvement in order to exhibit wide multiorder pass band response parallel to coupled slot line resonator-based 3-D FSS design approach has been recorded in [7].

This is to be noted that a very limited number of literature exists till date regarding the broadening of pass band as compared to the stop band enhancement. A 63% broaden −3 dB elliptical pass band filtering response has been achieved in [8] with three transmission poles with multilayer FSS configuration. Unlike the straightforward common method, third-order quasi elliptical pass band has also been achieved in [9]. A 75% bandwidth enhancement has been realized in [10] using metallic mesh-type complementary structure with skewed arrays of the modified triples. The employment of circular parasitic patch and two stage bend grid configurations to achieve more than 140% bandwidth has been discussed in [11]. A similar type of the cascading arrangement of three metallic layers separated by two dielectrics has been reported in [12] which contributes for the wide pass band of −3 dB bandwidth that extends from 6 to 19.25 GHz. The most recent attention toward the pass band enhancement technique is the incorporation of multiple interdigital resonators in multilayer arrangement [13]. The striking feature of fractal structures using the iterative process regarding the design miniaturization of unit cell is a straightforward analogy. The fascinating feature is the realization of multipole wider pass band frequency response which has also been comprehensively discussed in previous literature [14–18]. Along with the multiple transmission pole

realization, the roll-off and selectivity improvement are also highly desirable issues to achieve the sharp transmission response regarding wide or ultra-wide pass band realization. In this regard, 3-D FSS has been discussed in [15–17]. A completely new and flexible design approach to realize high order of filtering functionalities is the aperture-coupled patch resonator-based FSS design [19]. The slight curved surface of different types of radome, aircraft, or antenna sub-reflector configurations always emphasizes on the needs of conformable FSS arrangements on flexible materials [20, 21].

This paper introduces the cascading arrangement of symmetrical Minkowski island-shaped fractal FSS pair along with a spiral-shaped FSS at the middle layer. Each layer is composed of one ultrathin dielectric substrate ($0.00065\,\lambda_0$) with one-sided etched metallic arrangement. The optimized air gap coupling between each resonating layer is $0.012\,\lambda_0$ where λ_0 indicates the free space wavelength at the lower cut-off frequency. The spiral-shaped middle layer plays a crucial role regarding the sharp lower edge cut-off of the ultra-wide pass band that leads toward the significant enhancement of the pass band selectivity. The iteration procedure of Minkowski island fractal structure pair is mainly responsible for the pass band broadening at the upper cut-off edge of the frequency response.

Unit cell design of fractal geometry

The initial length is considered as L and then in iteration-1, the symmetrical truncation in terms of width and depth can be considered as $q{\times}L/3$ where q has been considered as iteration factor. This causes development of the Minkowski island fractal generator for each segment though the areas remain constant. Thus, the effective width after iteration-1 becomes $L{-}q{\times}L/3$. The first iteration of the fractal generator replaces every segment to the original square. The insertion of the slots in rectangular structure of iteration-0 introduces an additional capacitance. The innovative modified design procedure in iteration-2 geometry has been adopted other than the conventional symmetrical self-repeating iteration technique or self-similarity of the etched conductive layer where the asymmetrical width and depth ratio has been taken into account. In this optimized procedure, the vertical iteration factor $q/4$ and horizontal iteration factor $q/2$ have been considered to be quite different from the straight forward $q/3$ iteration factor of iteration level-2. Considering the modified iteration factor regarding width in proposed iteration-2, we may consider

$$W = [(L{-}q \times L/3) - (q/2) \times (3L{-}qL)/6]. \quad (1)$$

Owing to this novel fractal etching procedure, the diagonal asymmetry topology of the proposed fractal structure can be regarded as a more miniaturized configuration [22]. The perimeter variation of the effective fractal patch contributes to the enlarged inductive and additional capacitive feature.

Double-layered fractal structure

The stacking of using a double layer is unlike the traditional style where air gap coupling was rarely introduced. The iteration-0 to -2 symmetrical double-layered configuration development has been illustrated in Fig. 1a. A $0.25\,\lambda$ air gap cavity model between two symmetrical single-layered fractals with ultrathin FR-4 substrate provides a cascaded symmetrical double-layered structure where λ corresponds to the primary transmission zeros. Exciting −3 dB pass band broadening feature of upper cut-off frequency from 5.65 GHz of iteration-0 to 6.74 GHz iteration-2 has been exhibited with $0.25\,\lambda$ air gap coupling. The capacitive and inductive enhancement results for the shifting of transmission zeros toward lower spectral range closer to the pass band edge which consequently results in the pass band broadening with improved roll-off and the wide −10 dB second-order stop band characteristics are illustrated in Fig. 1b.

Relevance of the double-layered fractal structure

In early works, the meandered monopole exhibits multiband behavior with excellent angular stability [23, 24]. A pair of meandered FSS with air spacer has a significant role in widening of pass band characteristics for both the planar and conformal FSS array as discussed in [25]. However, these designs are incompetent to generate the wide pass band with enhanced fractional bandwidth.

A recent simplified design approach of [17] suggested that two symmetrical ring-shaped resonant layers with optimized air gap have excellent transmission performance for wide pass band in lower frequency range and better second-order reflection performance in stop band. However, pass band to stop band roll-off performance is very poor which has been enhanced in next development where inductive meandered grid has been included along with the ring-shaped resonator pair. The triple-layered cascaded hybrid resonating structure ultimately achieves UWB pass band and wide stop band characteristics with multiple transmission zeros. One noteworthy thing of the above discussion is the absence of pass band poles exhibition. Hence, the order of UWB pass band has not been discussed properly.

The replication of the geometry or the self-similarity in fractal configuration has obviously a great impact on wideband characteristics and the roll-off sharpness improvement. Previous literature [18] reveals a fascinating feature of fractal FSS where the order of wide pass band can be adjusted and the transmission poles can be controlled by simply changing the corresponding size of the fractal geometry. Furthermore, the structural symmetry of the fractal geometry significantly improves the polarization stability of the FSS. The proposed work regarding the exploration of fractal pair cascading also considers two approaches: broadening of the pass band and keeping closer separation between in band pole and out band zero which ensures the sharp and steep pass band roll-off characteristics. Several other literatures [26–28] also focused on the excellent angular stability of the fractal geometry which is a prime concern for this proposed work, particularly in EM stealth application. The multilayered cascaded hybrid resonating FSS may suffer due to the angular instability. However, the double-layered Minkowski island fractal layers along with spiral-shaped middle layer of the proposed work make FSS less sensitive to the angle of incident. Moreover, the stable response can also be achieved in conformal structure of the proposed FSS due to the inclusion of fractal geometries.

Insertion of the middle layer

In order to achieve the main aim of this proposed paper to generate more transmission pole in wide pass band characteristics with sharp selectivity, the proposed FSS in Fig. 2 presents a cascading arrangement of fractal pair geometry comprised of an additional middle coupling layer with regular spiral-shaped geometry on the ultrathin FR-4 substrate. The middle layer spiral-shaped resonator provides an additional transmission pole and zeros at

https://doi.org/10.1017/S1759078723000442 Published online by Cambridge University Press

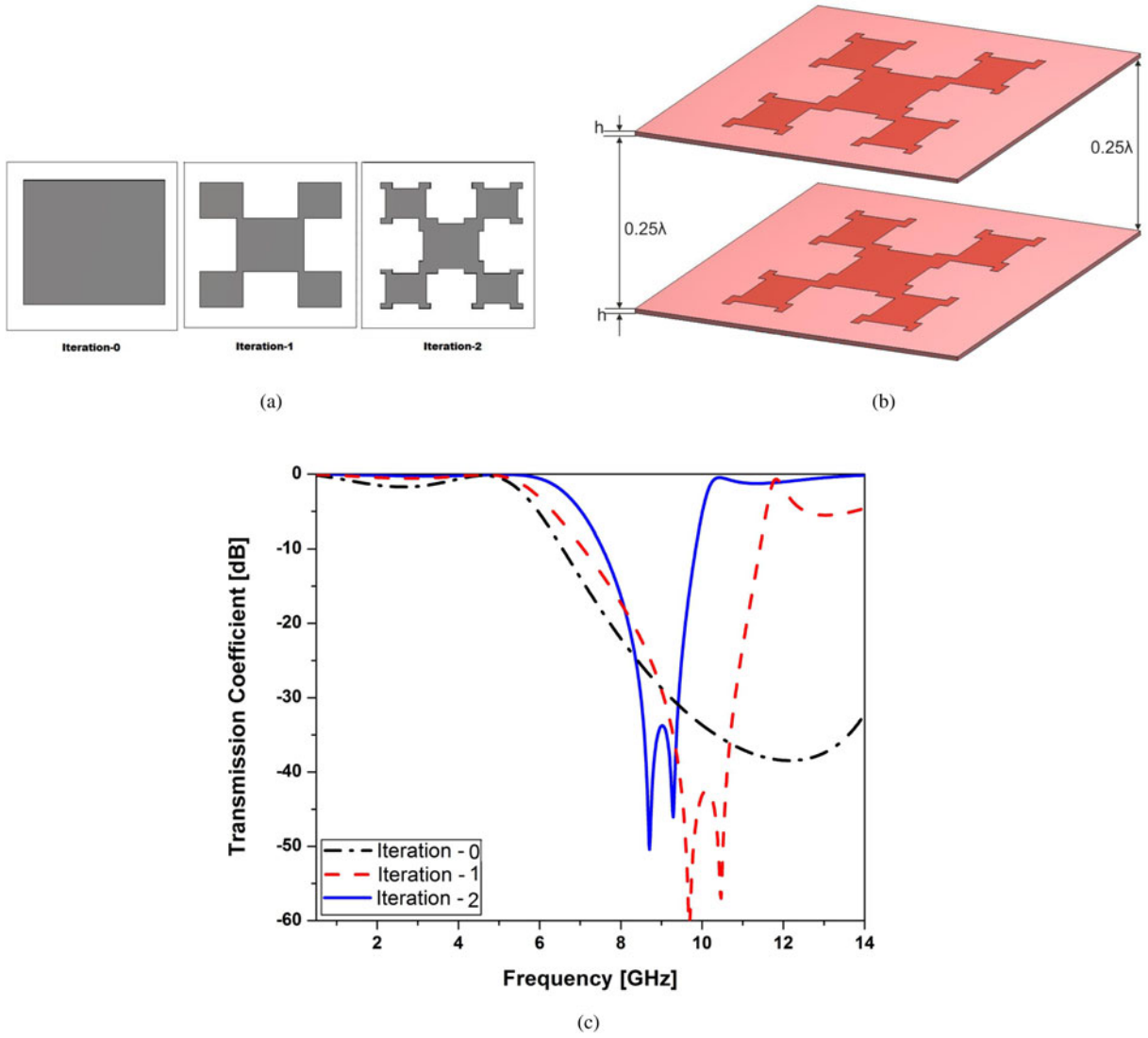

Figure 1. (a) Development of Minkowski island fractal geometry. (b) Double-layer side view of symmetrical iteration-2 fractal pair configuration with air gap separation. (c) Comparative frequency response of different iteration pair.

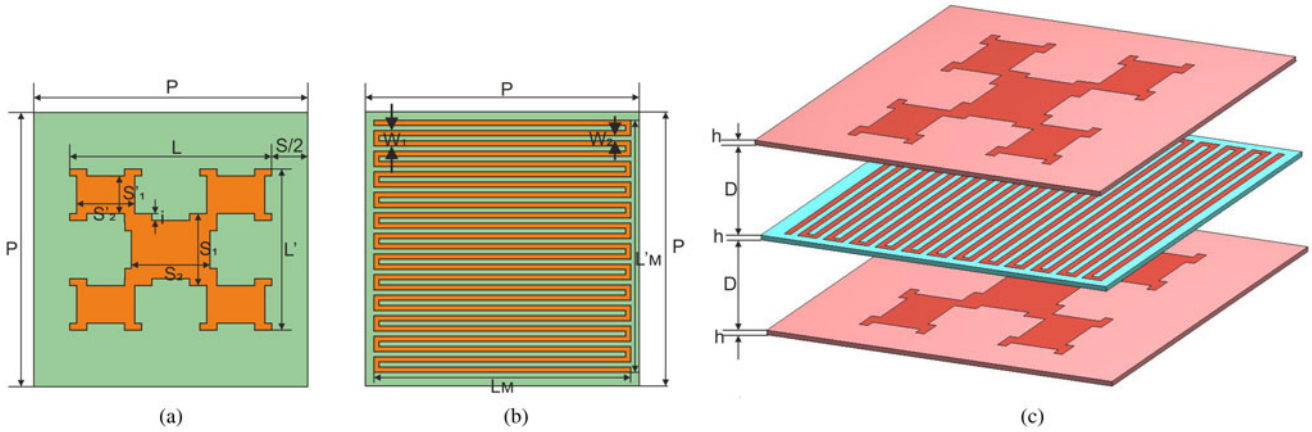

Figure 2. Proposed FSS geometry. (a) Top view of the top and bottom fractal configuration layer. (b) Top view of the middle spiral-shaped layer. (c) Side view of the proposed triple-layer FSS.

https://doi.org/10.1017/S1759078723000442 Published online by Cambridge University Press

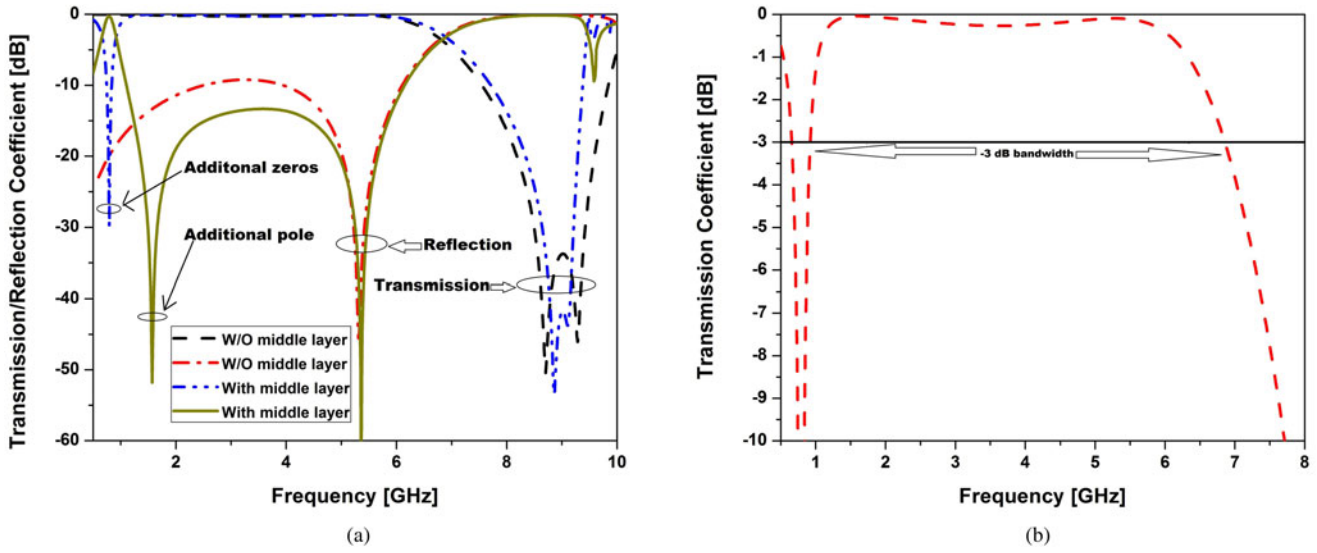

Figure 3. (a) Frequency response of double- and triple-layered FSS. (b) Selectivity performance of the proposed FSS.

the extreme lower spectral range. Figure 3a displays the reflection and transmission coefficients with and without the middle layer. It can be observed that two very close stop band transmission zero layers fall at 8.8 and 9.1 GHz along with one pass band transmission pole at 5.35 GHz without the insertion of middle layer. In the proposed FSS, the inclusion of the central layer just at the middle of the air gap generates the second-order UWB pass band filtering response that comprises of two transmission poles at 1.56 and 5.35 GHz with respect to the middle layer. The −3 dB pass band extends from 0.97 to 6.92 GHz. The transmission zeros realized at 0.81 GHz adjacent to the lower cut-off have significantly sharp characteristics. An excellent pass band steepness particularly closer to the lower cut-off frequency is realized that remarkably improves the overall pass band selectivity factor (SF) where

$$\mathrm{SF} = \frac{\mathrm{Bandwidth}_{-3\mathrm{dB}}}{\mathrm{Bandwidth}_{-10\mathrm{dB}}}. \tag{2}$$

The transmission coefficient of the proposed FSS in Fig. 3b illustrates the pass band that SF = 0.887 which is quite high as compared to the earlier reported values. The fractional bandwidth of the simulated result is also near about 151%. A wide and sharp stop band is also achieved with a spectral range of 7.7–9.4 GHz. The second-order stop band fractional bandwidth is 19.88%. Here, the simulation has been carried out by CST-MWS Solver. The dimensions of the parameters of the proposed FSS are listed in Table 1

Evolution of design synthesis

Each fractal patch element of the Minkowski island-shaped FSS pair of the top and bottom layers can be approximately modeled by series L_tC_t and L_bC_b lumped resonating element correspondingly. The LC equivalent circuit of the ultrathin substrate can be ignored as the inductive and capacitive effect of substrate is directly proportional to the thickness of the substrate. The air gap separation can be modeled as the transmission line with a characteristic impedance of $Z_0 = 377\,\Omega$. The full-wave simulation of Minkowski island-shaped FSS pair with $\lambda/4$ air gap separation has been explored initially where λ corresponds to the first transmission zeros. The realization of the perfect coupling is possible with $\lambda/4$ separation. The simulation results of CST-MWS EM solver reveals the existence of two successive transmission zeros with the presence of one transmission pole. The air gap separation has a significant role regarding the pass band stability mainly due to the proximity of the upper cut-off frequency. It can be observed in Fig. 4 that the reduced air gap from $\lambda/4$ to $\lambda/16$ severely deteriorates the pass band response. The reflection and transmission coefficient responses near the pole degrade sharply due to the loosely coupled layers where transmission coefficient is declining below −3 dB and similarly the reflection coefficient is well above −10 dB with the increasing air gap.

The iteration increment of Minkowski island fractal structure has a crucial role regarding the change of the effective width of the fractal plane. As the iteration increases, the effective width degrades and thereby the inductive effect enhancement occurs so that the L_tC_t and L_bC_b in fractal metallic patch geometry can

Table 1. Optimized dimension of the proposed FSS parameters

	P	L	L'	S	S_1	S_2	S'_1	S'_2	i
Top/bottom layer	16	11.79	9.40	8.42	4.20	4.60	2.20	3.40	0.40
Middle layer	P	L_m	L'_m	W_1	W_2	h	D		
	16	15	14.70	0.90	0.30	0.2	3.9		

https://doi.org/10.1017/S1759078723000442 Published online by Cambridge University Press

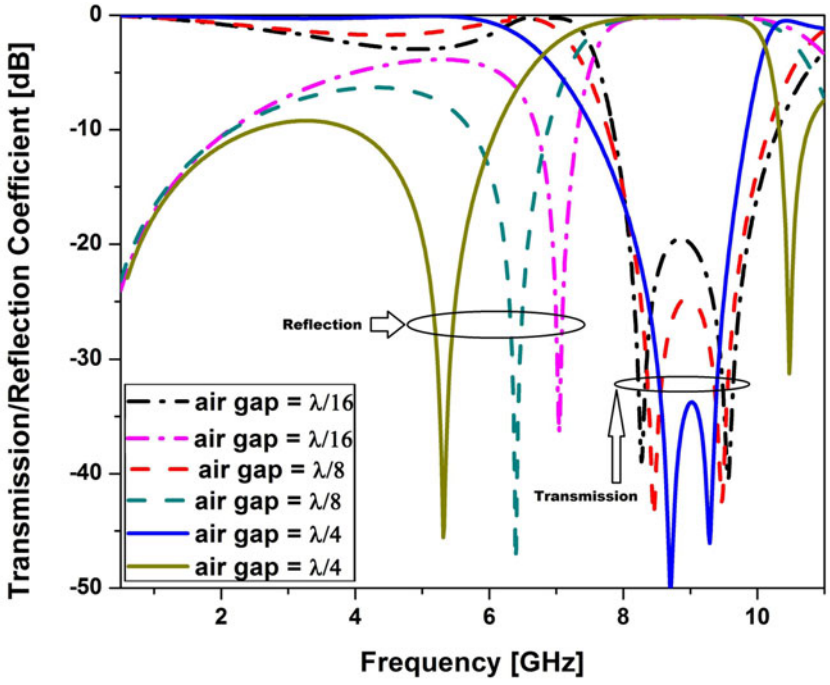

Figure 4. Influence of air gap separation in frequency response of the double-layered symmetrical Minkowski island fractal pair.

be mapped as

$$L_t = L_b = \mu_0 \mu_{eff} \ln\left(\frac{1}{\sin\left(\frac{\pi W}{2P}\right)}\right) \tag{3}$$

and

$$C_t = C_b = \mu_0 \mu_{eff} \ln\left(\frac{1}{\sin\frac{\pi S}{2P}}\right). \tag{4}$$

According to the general guideline, W is the effective width of the proposed fractal geometry which has been derived from equation (5), S is the separation between two unit cells and P is the period of the unit cell structure in fractal FSS array. The major concentration of the surface current distribution also confirms the fascinating feature of the modified fractal geometry for iteration-2. The transmission and reflection coefficient response of the dual-layer Minkowski island fractal pair equivalent circuit model (ECM) model with air gap separation has been validated by the multiple simulation of ADS solver as shown in Fig. 5. The extracted parametric value has been tabulated in Table 2

The middle layer spiral-shaped meandering grid contributes toward the parallel L_1C_1 configuration in series connection with L_2. The etched spacing between horizontal narrow metallic strips has been modeled as the capacitive effect C_1 parallel to the vertical narrow meandered strip as inductive effect L_1. The parallel approximated successive L_1C_1 resonating circuit connected with each other by using the narrow horizontal metallic grid mapped as L_2. The impedance (Z) of the middle layer geometry has been constructed in ECM as

$$Z = \frac{j\omega L_1 + j\omega L_2\left(1 - \omega^2 L_1 C_1\right)}{\left(1 - \omega^2 L_1 C_1\right)}. \tag{5}$$

Hence, the transmission zeros can be expressed as

$$\omega_z = \sqrt{\frac{(L_1 + L_2)}{L_1 L_2 C_1}}. \tag{6}$$

The transmission pole can be expressed as

$$\omega_p = \frac{1}{\sqrt{L_1 C_1}} \tag{7}$$

The comprehensive operative mechanism of the above-mentioned meandered spiral-shaped middle layer has been assisted by the parametric study of the structural variation as shown in Fig. 6. The noteworthy effect is the etched spacing between narrow horizontal parallel strips which produces strong capacitive effect with closer gap. As the gap increases, the capacitive effect declines sharply. In spite of the slight increment of L_1, it effectively shifts ω_p toward higher frequency range. However, the shifting of ω_z is slightly lower due to the presence of large L_2. An excellent coherence of transmission coefficient response between simulated and calculated ECM model transmission coefficient response regarding proposed triple-layered FSS (including the middle layer) can be observed in Fig. 7. The approximated L_1, L_2, and C_1 values are shown in Table 2.

Conformal feature

In real-time application, the conformal behavior of FSS becomes noteworthy owing to their applicability in radome, aircraft, or

https://doi.org/10.1017/S1759078723000442 Published online by Cambridge University Press

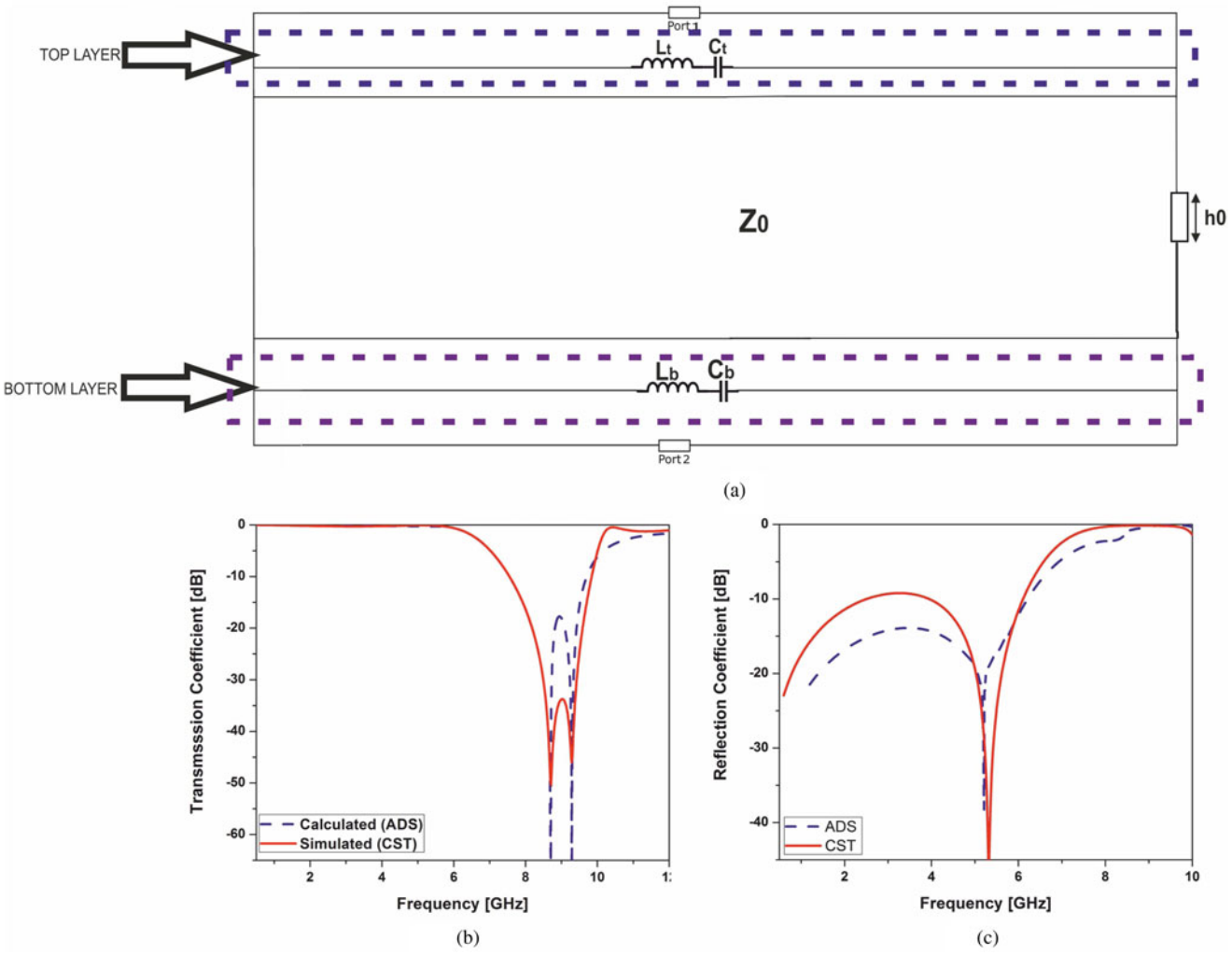

Figure 5. (a) Equivalent Circuit model of double-layered Minkowski island fractal pair FSS. (b) Comparative transmission coefficient and (c) reflection coefficient of double-layered FSS at CST-MWS and ADS.

parabolic sub-reflector. In straightforward manner, the conformal and planar both should exhibit the similar characteristics. However, some noticeable cornerstone like the operating frequency and the bandwidth deviation inherently discriminates the planar and bending feature of FSS [29]. Nevertheless, the partial deviation of conformal characteristics within the limited range may be justified for the aforesaid practical application. In this article, CST-MWS EM solver has been employed to investigate the conformal behavior of the proposed FSS, 4×4 lattice of the triple-layer unit cell as shown in Figs 8a and 8b. A different bending degree with vacuum cylindrical radius has been considered. In order to realize the structural symmetry and the suppression of higher order modes, the cylindrical curved structure is held to the open boundary along Z-axis in X-Y plane with added space. In curved configuration, the coupling between array elements is declining noticeably which eventually improves the roll-off sharpness. Other conceptual observation regarding the curved configuration is the large incident angle at the nearby unit cell array element on the curved surface. These results in the noticeable development of phase difference in the magnetic field where the plane wave is incident are concerned, which ultimately reduces the fractional bandwidth. Figures 8c and 8d illustrate the simulated transmission coefficient response of the proposed structure with varying cylindrical curvature in TE and TM polarization. As observed, the transmission response in TM mode has better selectivity as compared to TE. It can be perceived from Fig. 8c that the secondary pass band pole of TE polarization is shifted significantly toward the higher frequency range with the increment of the bending angle. In contrary, the slight shifting of stop band zeros toward the lower frequency consequently makes a closer separation between falling edge pass band transmission pole and adjacent stop band zeros that ultimately leads to the roll-off improvement and sharp selectivity. The frequency

Table 2. Parameters of the equivalent circuit model

Parameter	L_t	C_t	L_b	C_b	L_C
Value	4.26 nH	78.6 fF	4.38 nH	67.1 fF	1.02 nH
Parameter	C_C	L_1	C_1	L_2	
Value	0.61 pF	0.8 nH	45.72 pF	4.73 nH	

https://doi.org/10.1017/S1759078723000442 Published online by Cambridge University Press

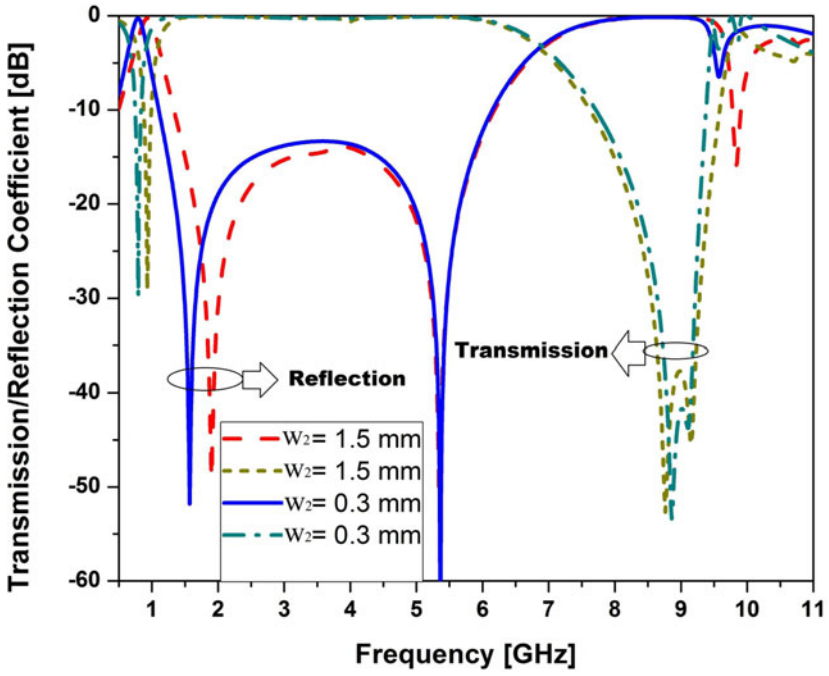

Figure 6. Influence of the spiral-shaped FSS modification on the primary in band transmission pole and out band transmission zeros.

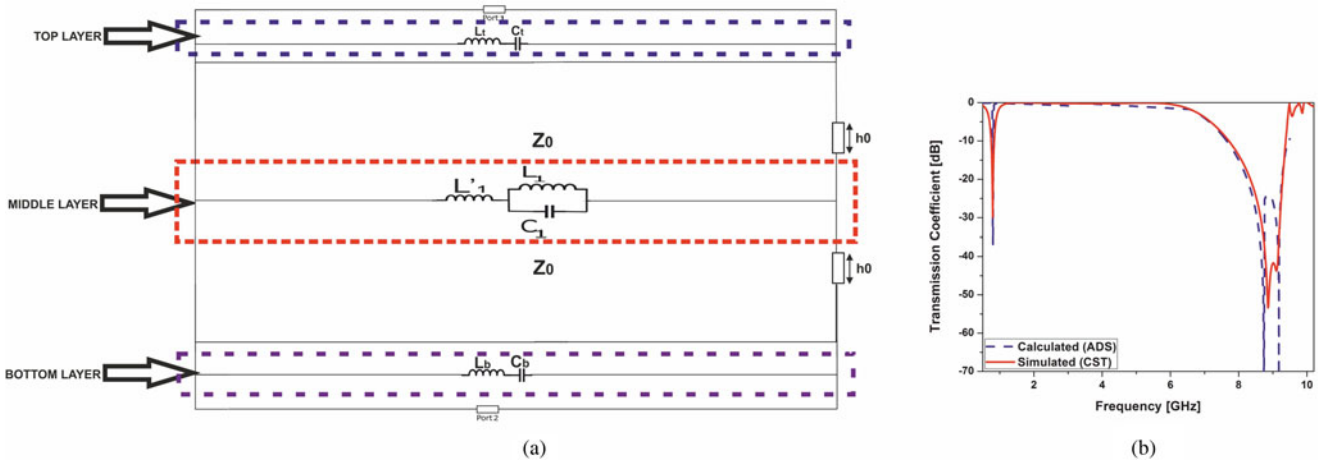

Figure 7. (a) Equivalent circuit model of the proposed triple-layered FSS. (b) Transmission coefficient of the proposed triple-layered FSS at CST-MWS and ADS.

ratio between the pass band transmission poles to nearby transmission zeros adjacent to the higher cut-off pass band edge reduces from 1.66 to 1.37. However, the fractional bandwidth deviation regarding pass band and stop band is almost negligible with different radius of curvature. The above-mentioned spectral observation clearly indicates the stability of the conformal characteristics.

Angular stability

The simulated transmission coefficients of the proposed triple-layered planar FSS in both TE and TM polarization modes under different oblique incidents are illustrated in Fig. 9. Remarkable stability of pass band and stop band response can be observed from 0° to 60° except a small flicker around 8.4 GHz, particularly in TE mode with higher angular incident angle. This problem may arise due to the structural asymmetry of the middle layer and the air gap. However, the flat characteristics of transmission coefficient less than −1 dB in the entire pass band (0.96–6.92 GHz) can be observed. Transmission coefficient of TM response for $0^{\circ} \leq \theta \leq 60^{\circ}$ also exhibits the excellent pass band characteristics well above −3 dB for the spectral range 0.96–7.15 GHz. The selectivity (SF = 0.935) of TM pass band response is quite excellent as compared to the TE pass band selectivity (SF = 0.872). Besides, the stop band response lowers than −10 dB in between the spectral range of 7.45–9.61 GHz with negligible deviation for both the polarization modes observed. Moreover, another significant issue is the negligible

https://doi.org/10.1017/S1759078723000442 Published online by Cambridge University Press

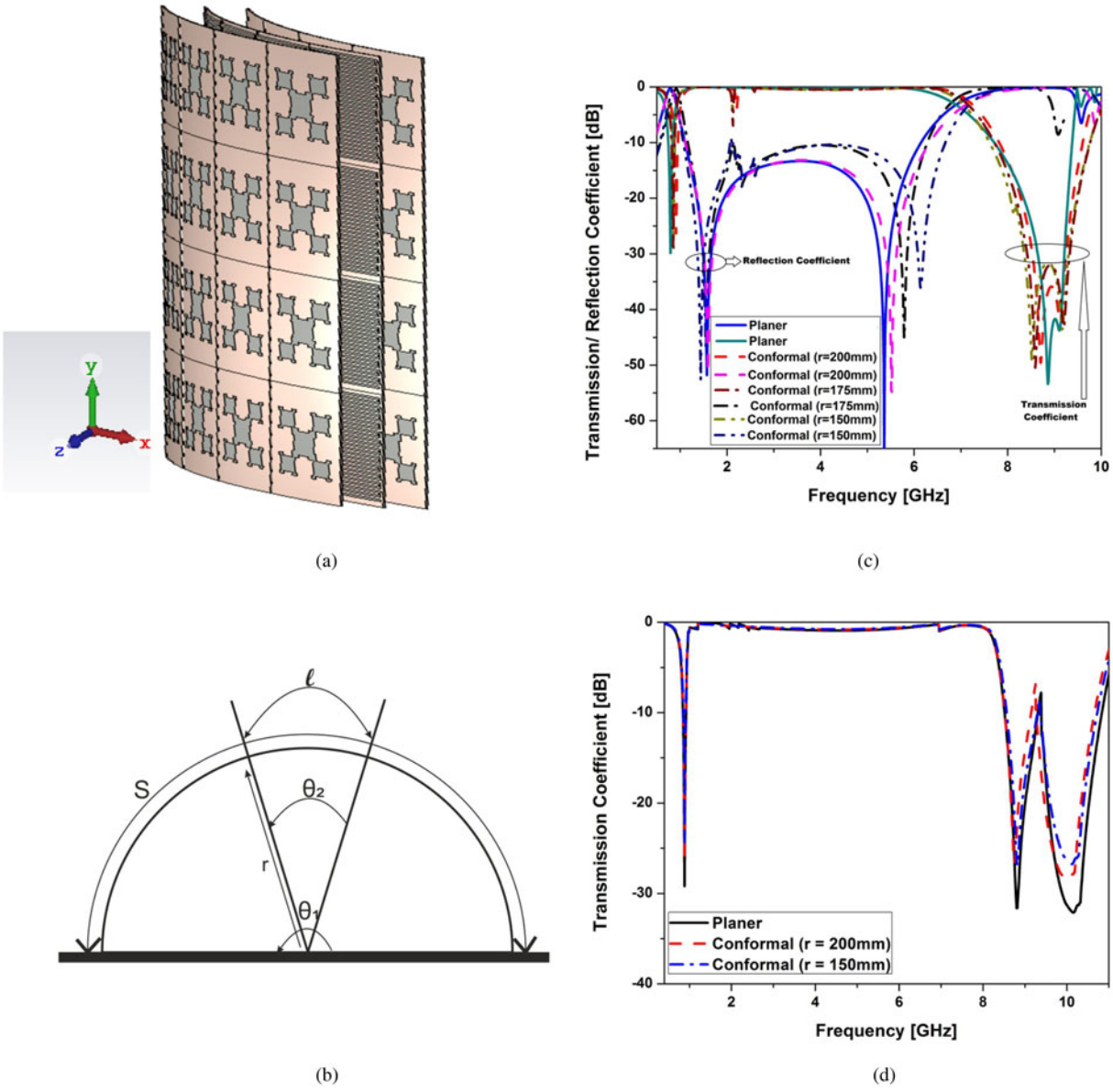

Figure 8. (a) Conformal structure of 4 × 4 proposed FSS lattice. (b) 2D view of conformal structure with cylindrical bending. (c) Frequency response of the proposed FSS with varying radius of curvature in TE mode. (d) Frequency response of the proposed FSS with varying radius of curvature in TM mode.

bandwidth deviation for both the TE and TM polarizations with large oblique incident angle along with a sharp pass band selectivity that validates the angular stability potential of the proposed FSS geometry.

Modified cascading arrangement to reduce polarization sensitivity

The middle layer of the proposed FSS has the spiral-shaped geometry and due to the lack of symmetrical arrangement of this unit cell design, the proposed triple-layer cascaded FSS structure exhibits the polarization sensitivity. Therefore, a significant change of transmission characteristics can be seen with varying polarization angle. The transmission response deviation with respect to the increasing polarization angle is significantly high, particularly at the higher pass band spectral coverage region with numerous spurious resonances as illustrated in Fig. 10. Besides, the sharp deterioration of the lower frequency transmission zero with increasing polarization angle can also be observed which clearly indicates the polarization sensitivity due to the middle layer.

Since the polarization independence of FSS is the crucial characteristic for extensive application and practical feasibility, a possible design modification can be explored in the next development phase in order to obtain the diminutive polarization sensitivity. A new and simplified cascading strategy has been adopted regarding the modified design which comprises of two ultrathin sandwiched middle layers with similar meandered spiral geometry in quadrature rotation instead of single layer with optimized air gap inside the Minkowski island fractal FSS pair as illustrated in Fig. 10c. The inclusion of additional spiral-shaped layer in qudrature angular rotation along with the existing middle layer evidently changes the coupling effect. Therefore, in the modified four-layered cascaded structure, the 0.10 λ_0 air gap separation between the middle layers has been maintained as compared to the triple-layer

https://doi.org/10.1017/S1759078723000442 Published online by Cambridge University Press

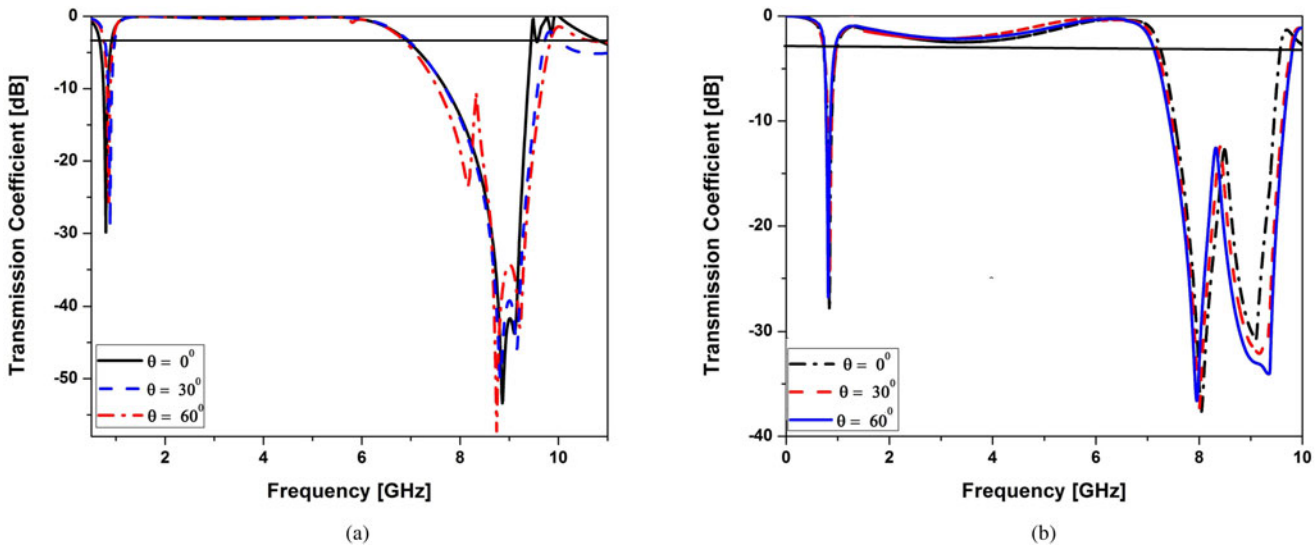

Figure 9. Simulated transmission coefficient of the proposed FSS for different incident angles at (a) TE polarization and (b) TM polarization.

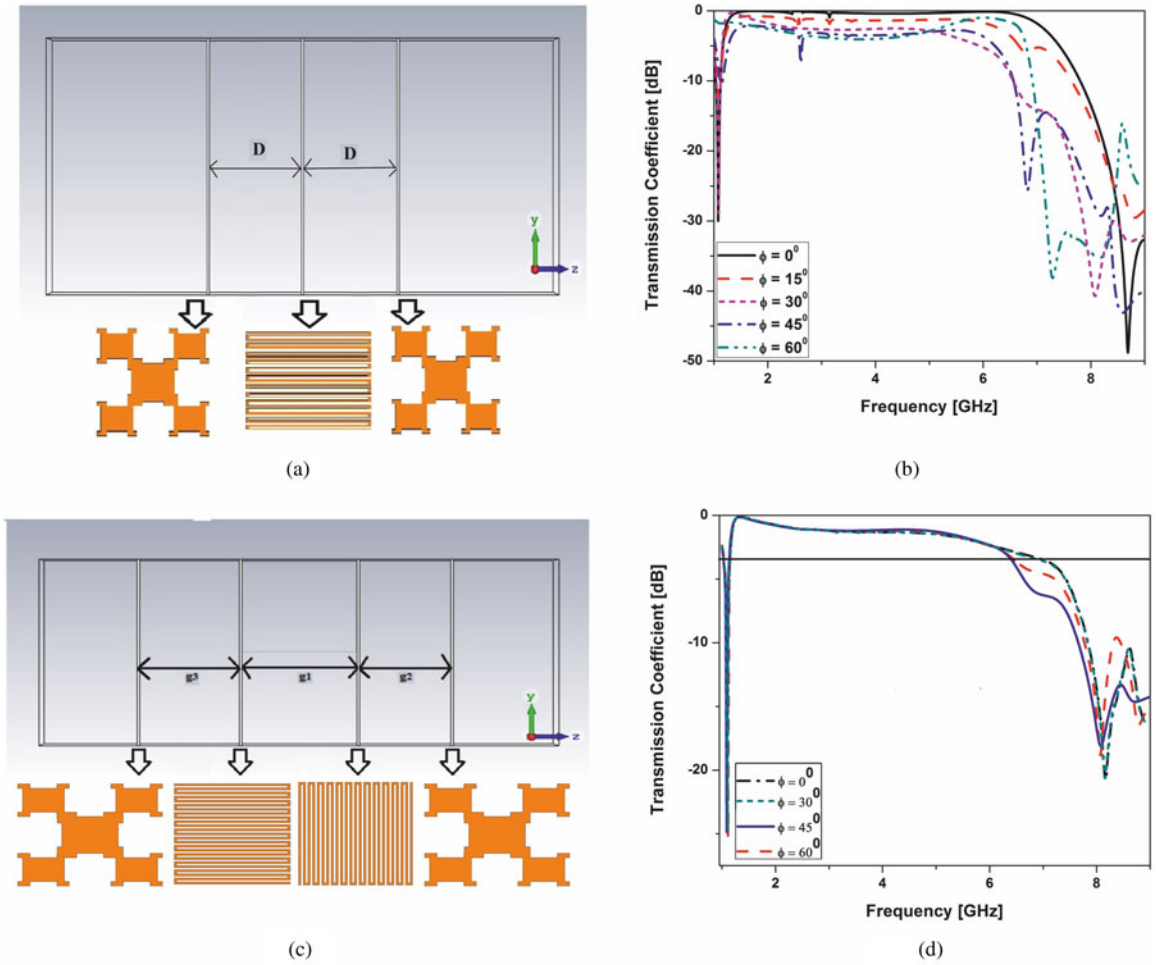

Figure 10. (a) CST-MWS model of the proposed triple-layered cascaded FSS ($D = 3.9$ mm). (b) Transmission coefficient response of triple-layered FSS for different polarization angles under normal incidence. (c) CST-MWS model of the modified quad-layered cascaded FSS ($g_1 = 4.2$ mm, $g_2 = 2.1$ mm, $g_3 = 2.1$ mm). (d) Transmission coefficient response of quad-layered FSS for different polarization angles under normal incidence.

https://doi.org/10.1017/S1759078723000442 Published online by Cambridge University Press

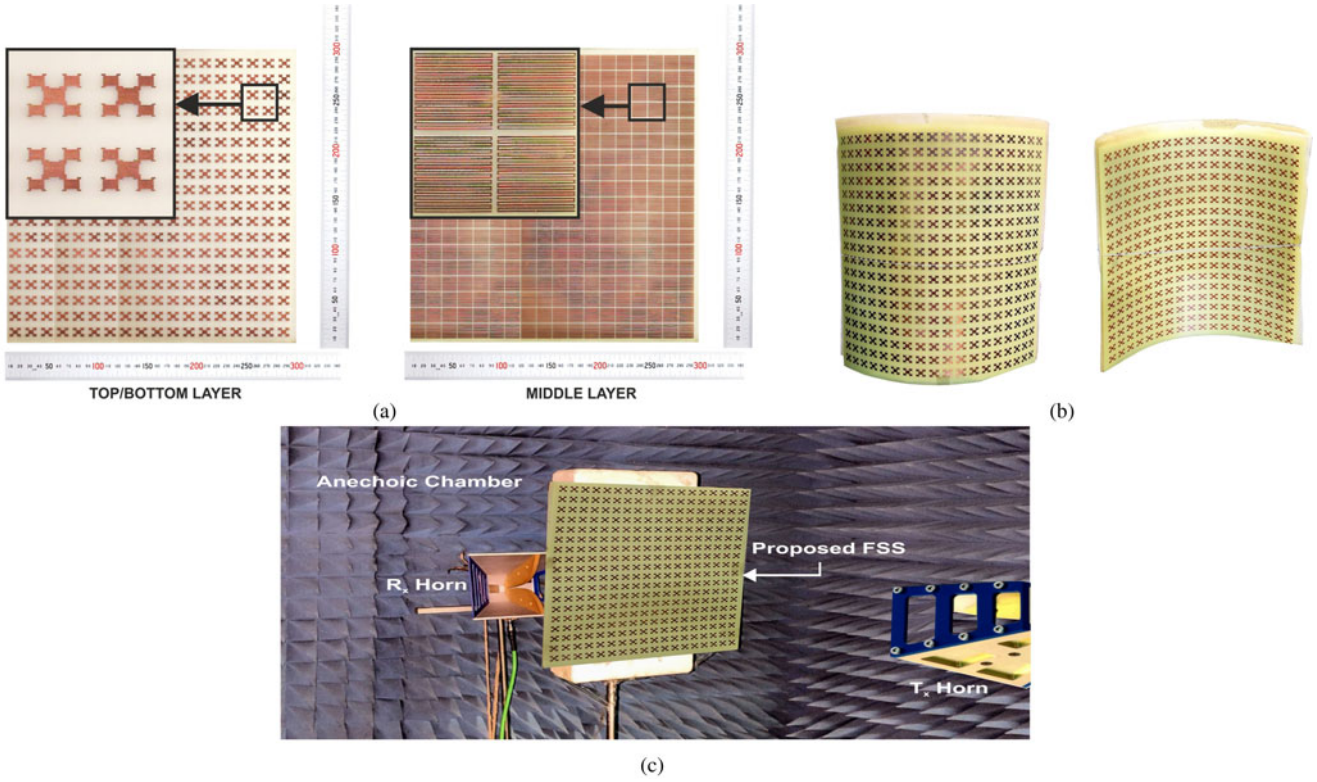

Figure 11. (a) Fabricated planar prototype of Minkowski island-shaped fractal and spiral-shaped configuration. (b) Conformal structure of the proposed triple-layered FSS. (c) Free space measuring setup for planar FSS at 40° incidence angle.

cascaded geometry where the optimized symmetrical air gap between the successive layers is $0.125\,\lambda_0$. Here λ_0 indicates the free space wavelength of first transmission zero. Due to the rotational geometry, the quasi symmetrical feature can be achieved which ensures the reduced polarization sensitivity of the four-layered cascaded FSS. The transmission coefficient response of the modified cascaded arrangement exhibits better coherence with different polarization angle as compared to the triple-layered transmission response as illustrated in Fig. 10d. Although the insertion of additional layer in quadrature orientation attenuates the pass band response, the effective transmission response is well above the −3 dB threshold value.

Experimental verification

The transmission and reflection coefficient measurements of the proposed cascaded 300×300 mm^2 triple-layered fabricated prototypes are carried out by two dual ridge broad band horn antenna setup pair of measurement range 800 MHz to 18 GHz which are connected to a network analyzer (Keysight N9918A Field fox) inside the anechoic chamber as shown in Fig. 11. The transmitting and receiving horn antenna have been calibrated initially with the optimized separation distance greater than or equal to $2D^2/\lambda$ where D is the maximum dimension of the antenna and λ denotes the operating wavelength [30]. The fixture is arranged in such a way that it ensures the transmission and reflection of adequate amount of radio wave through the planar aperture area of FSS array. The transmission and receiving antenna angular spacing has been rearranged further in order to achieve the proper reflection from the conformal structure.

The measured frequency response of the planar and conformal FSS is illustrated in Figs 12a and 12b, respectively. The transmission and reflection coefficients depict the second-order UWB pass band and second-order wide stop band filtering responses. The −3 dB pass band range is extended from 0.96 to 6.97 GHz whereas the stop band range is 8.02–9.97 GHz. SF of the measured pass band is about 0.887. Two in-band transmission poles can be observed. In a similar way, the conformal structure of the proposed FSS array has −3 dB UWB pass band ranging from 1.0 to 7.2 GHz and the spectral range of −10 dB stop band characteristics is 8.1–9.3 GHz. Moreover, the closer resemblance of pass band selectivity between planar and conformal configuration can also be observed with conformal SF = 0.885. The pass band response in both the planar and the conformal configuration is almost flat and more stable with an insertion loss of −0.76 and −1.55 dB correspondingly at the center frequency of the pass band. The envelope of the experimental outcome of planar and conformal configuration is in coherence with the simulated results. The incident case under TE polarization is shown in Fig. 13. Despite some simulated and experimental ripples, particularly near the falling edge of the pass band characteristics of TE mode at $\theta = 45^{\circ}$, the overall pass band and stop band responses are in good agreement with sharp pass band selectivity. Although the strong air gap coupling between the layers may generate additional resonance effect with increasing oblique incidence at TE mode, the angular stability can clearly be observed over the wide oblique incident angle. Owing to the noticeably stable conformal characteristics and significantly wide angular

https://doi.org/10.1017/S1759078723000442 Published online by Cambridge University Press

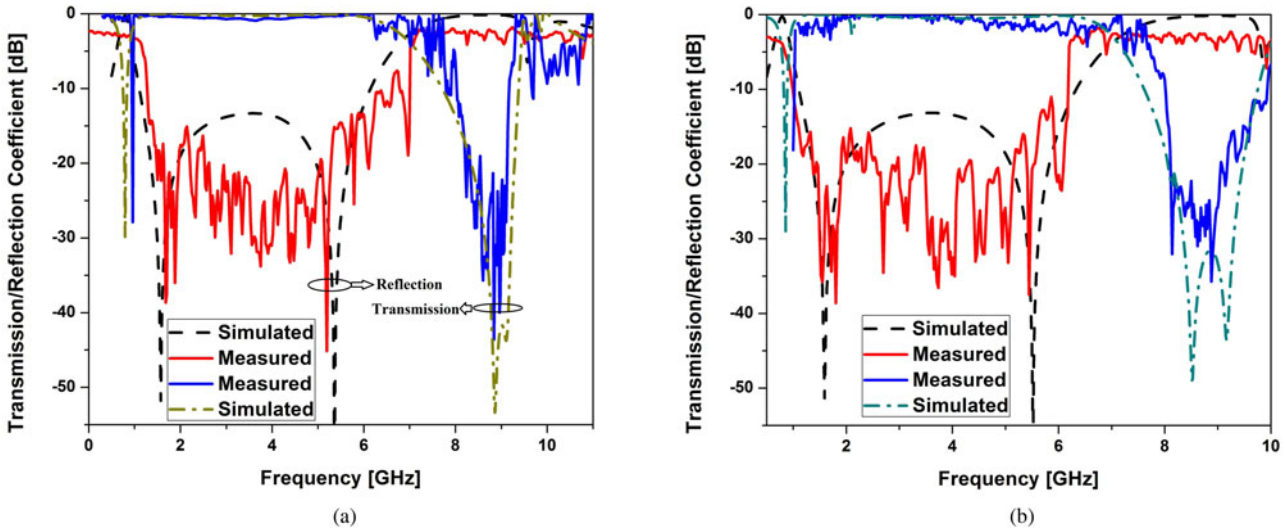

Figure 12. Measured frequency response of (a) planar and (b) conformal configuration.

and polarization stability, the ultra-wide pass band spectral range of the proposed FSS is predominantly suitable for the EM stealth in 0.9–1.8 GHz GSM band, 2.10–2.14 GHz wireless medical telemetry band, 2.4–2.5 and 4.9–5.8 GHz WLAN band, 3.4–3.7 and 4.4–4.9 GHz sub-6 GHz 5 G band, and 3.7–4.2 GHz C band. Furthermore, a strong shielding effect also has been provided by the proposed FSS which covers lower *X* band frequency range. Figure 14 illustrates the precise identification of the aforesaid narrow band employability within the spectral coverage of the proposed FSS in EM stealth and EM shielding.

Comparison with the earlier reported works

Table 3 illustrates the performance comparison of the proposed FSS with previously reported structures. The comparison has been focused on unit cell dimension and thickness in terms of free space wavelength (λ_0) at lower cut-off frequency of UWB pass band characteristics. Besides, other focusing issues are the FBW of pass band and stop band characteristics, pass band selectivity, angular stability, and conformal behavior where the proposed UWB FSS clearly indicates its excellence.

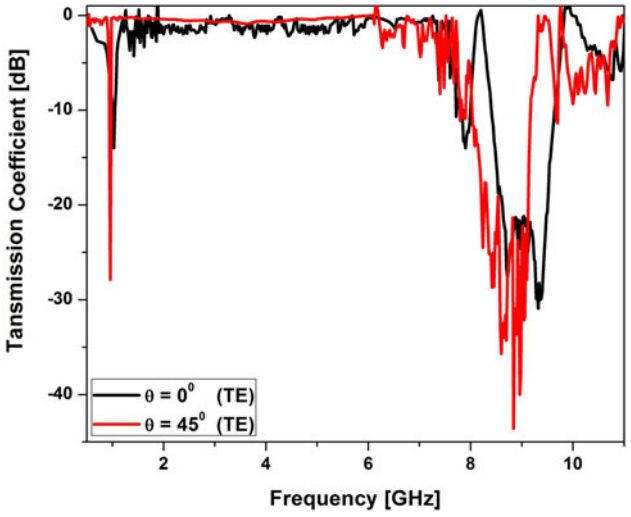

Figure 13. Simulated versus measured frequency response at various incident angles under TE polarization.

Conclusion

A novel approach of pass band broadening with improved selectivity using sub-wavelength fractal-shaped hybrid resonating cascaded geometry with optimized air gap is presented in this paper. The cascaded fractal-shaped symmetrical resonating pair with air gap coupling instigates the enhancement of the upper cut-off of pass band of the transmission characteristics with improved one-sided roll-off. It also contributes toward the wide stop band (18.4%) with two closely spaced transmission zeros. However, the reflection performance regarding pass band is quite inferior owing to the absence of transmission pole toward the lower frequency range. The spiral-shaped coupling layer inclusion at the middle layer contributes to the additional transmission zeros and poles at the lower edge of the pass band that leads toward the flat (−3 dB) ultra-wide pass band transmission characteristics (151.3%) and significantly improves (−10 dB) reflection response with two in band transmission poles. A steep transition and sharp cut-off for ultra-wide pass band response of the proposed triple layer cascaded structure is particularly due to the introduction of two out band transmission zeros at the vicinity of lower and upper cut-off edges. The ECM is also presented to validate the emergence of a highly selective ultra-wide flat pass band with two transmission poles along with the second-order wide stop band. Furthermore, the stable transmission and reflection responses are also illustrated for the conformal structure. A comprehensive investigation regarding the stability in large incident angle variation for TE and TM polarizations exhibits the better angular stability. Moreover, the proposed design lacks polarization independence, and a modified design has been suggested in order to suppress the polarization sensitivity of the proposed cascaded structure. Finally, the aforesaid fascinating features regarding parametric improvement are successfully validated by the measured results which thereby ensure a promising employability of the proposed ultra-wide pass band FSS in case of EM stealth in GSM band, wireless medical telemetry band,

https://doi.org/10.1017/S1759078723000442 Published online by Cambridge University Press

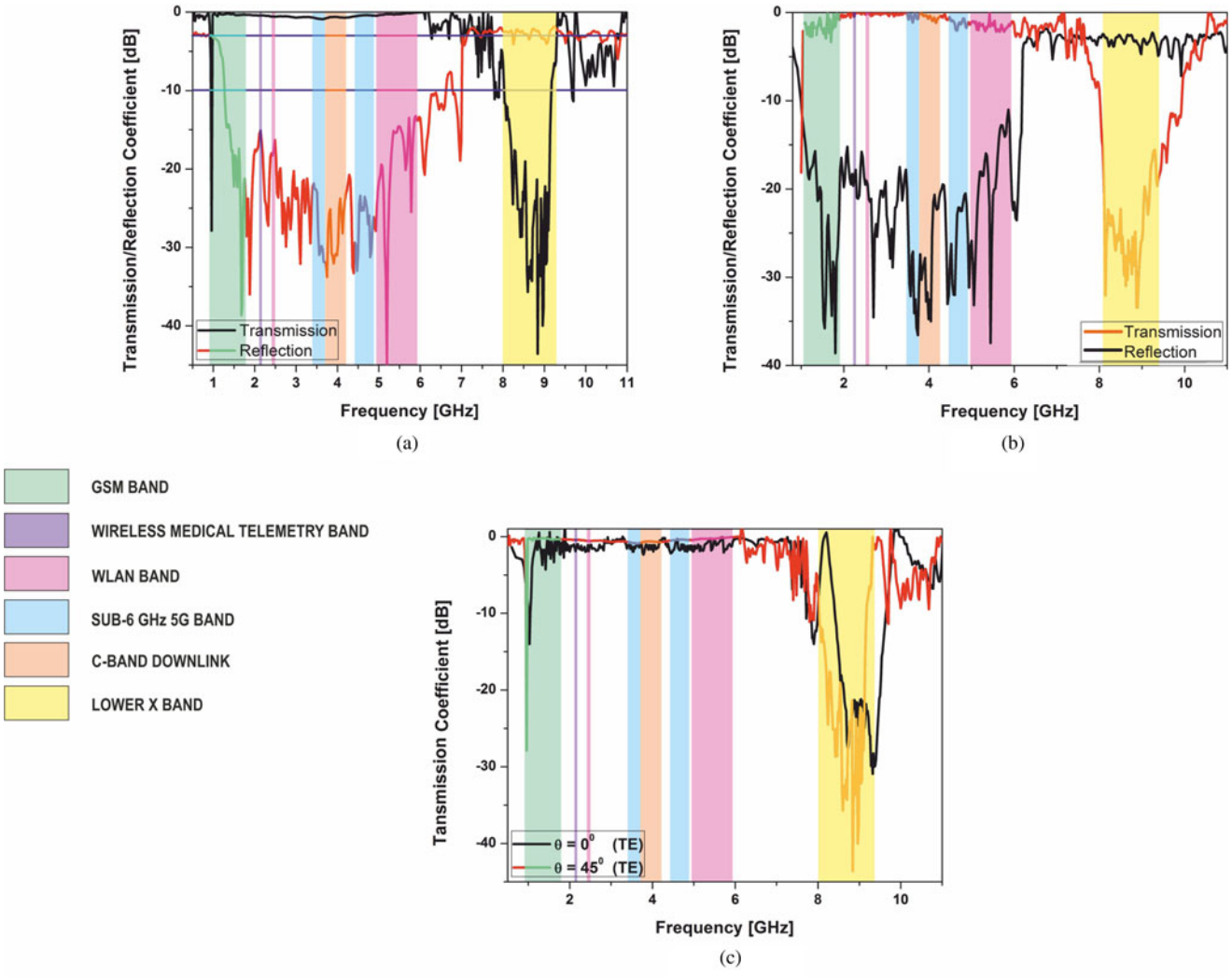

Figure 14. Spectral coverage of GSM, wireless medical telemetry, WLAN, sub-6 GHz 5G, and C bands for the frequency response of (a) planar structure at normal incidence, (b) conformal structure at normal incidence, and (c) planar structure at 45° incident angle.

Table 3. Comparative study of the proposed FSS with previously reported works

References	Unit cell size	Effective thickness	FBW(−3 dB pass band)	FBW(−10 dB stop band)	Selectivity factor	Angular stability (transmission coefficient ≥−3 dB)	Conformal feature
Ref.[7]	$0.16\,\lambda_0 \times 0.16\,\lambda_0$	$0.544\,\lambda_0$	123%	NA	0.882	40°	NA
Ref.[8]	$0.219\,\lambda_0 \times 0.219\,\lambda_0$	$0.087\,\lambda_0$	63%	NA	0.822	40°	NA
Ref.[11]	$0.25\,\lambda_0 \times 0.25\,\lambda_0$	$0.038\,\lambda_0$	140.5%	NA	0.728	60°	NA
Ref.[12]	$0.117\,\lambda_0 \times 0.117\,\lambda_0$	$0.039\,\lambda_0$	105%	NA	0.817	30°	NA
Ref.[13]	$0.20\,\lambda_0 \times 0.20\,\lambda_0$	$0.162\,\lambda_0$	111%	NA	0.715	NA	NA
Ref.[14]	$0.20\,\lambda_0 \times 0.20\,\lambda_0$	$0.103\,\lambda_0$	87.4%	NA	0.738	30°	NA
Ref.[15]	$0.27\,\lambda_0 \times 0.27\,\lambda_0$	$0.349\,\lambda_0$	97.6%	NA	0.931	30°	NA
Ref.[16]	$0.105\,\lambda_0 \times 0.105\,\lambda_0$	$0.257\,\lambda_0$	26.3%	57.4%	0.636	60°	NA
Ref.[17]	$0.026\,\lambda_0 \times 0.026\,\lambda_0$	$0.283\,\lambda_0$	155.7%	67.9%	0.889	45°	NA
This work	**$0.049\,\lambda_0 \times 0.049\,\lambda_0$**	**$0.026\,\lambda_0$**	**151.3%**	**18.4%**	**0.887**	**45°**	**Yes**

https://doi.org/10.1017/S1759078723000442 Published online by Cambridge University Press

WLAN band, sub-6 GHz 5 G band, and C band down link. In contrary to that, it also inhibits the frequency band 8–9.3 GHz which leads toward employability of the proposed FSS for lower *X* band shielding.

Acknowledgments. The authors would like to acknowledge Dr. Partha Pratim Sarkar of DETS, Kalyani University and Prayukti Bhawan, University of Jadavpur, India for the measurements.

Financial support. None.

Conflict of interest. None.

References

1. **Munk BA** (2005) *Frequency Selective Surfaces: Theory and Design*. Hoboken, New Jersey, USA: Wiley.
2. **Al-Joumayly M and Behdad N** (2009) A new technique for design of low-profile, second-order, bandpass frequency selective surfaces. *IEEE Transactions on Antennas and Propagation* **57**, 452–459.
3. **Li B and Shen Z** (2013) Synthesis of quasi-elliptic band pass frequency-selective surface using cascaded loop arrays. *IEEE Transactions on Antennas and Propagation* **61**, 3053–3059.
4. **Hussein M, Zhou J, Huang Y and Al-Juboori B** (2017) A low-profile miniaturized second-order bandpass frequency selective surface. *IEEE Antennas and Wireless Propagation Letters* **16**, 2791–2794.
5. **Wu W, Liu X, Cui K, Ma Y and Yuan Y** (2017) An ultrathin and polarization-insensitive frequency selective surface at Ka-band. *IEEE Antennas and Wireless Propagation Letters* **17**, 74–77.
6. **Liu N, Sheng X, Zhang C and Guo D** (2019) Design and synthesis of band-pass frequency selective surface with wideband rejection and fast roll-off characteristics for radome applications. *IEEE Transactions on Antennas and Propagation* **68**, 2975–2983.
7. **Li H, Li B and Zhu L** (2020) Wideband bandpass frequency-selective structures on stacked slotline resonators: proposal and synthetic design. *IEEE Transactions on Antennas and Propagation* **68**, 7068–7078.
8. **Lv Q, Jin C, Zhang B and Mittra R** (2019) Wide-passband dual-polarized elliptic frequency selective surface. *IEEE Access* **7**, 55833–55840.
9. **Chen G-W, Wong S-W, Li Y, Chen R-S, Zhang L, Rashid AK, Xie N and Zhu L** (2021) High roll-off frequency selective surface with quasi elliptical band pass response. *IEEE Transactions on Antennas and Propagation* **69**, 5740–5749.
10. **Xu N, Gao J, Zhao J and Feng X** (2015) A novel wideband, low-profile and second-order miniaturized band-pass frequency selective surfaces. *Aip Advances* **5**, 077157.
11. **Tang Z, Zhan J, Zhong B, Chen L and Zuo G** (2022) An ultra-wideband frequency selective surface with high stability for electromagnetic stealth. *Journal of Electromagnetic Waves and Applications* **36**, 141–153.
12. **Zhou H, Qu SB, Wang JF, Lin BQ, Ma H, Xu Z and Peng WD** (2012) Ultra-wideband frequency selective surface. *Electronics Letters* **48**, 11–13.
13. **Wang L, Liu S, Kong X, Zhang H, Yu Q and Wen Y** (2019) Frequency-selective rasorber with a wide high-transmission passband based on multiple coplanar parallel resonances. *IEEE Antennas and Wireless Propagation Letters* **19**, 337–340.
14. **Anwar RS, Wei Y, Mao L and Ning H** (2019) Miniaturised frequency selective surface based on fractal arrays with square slots for enhanced bandwidth. *IET Microwaves, Antennas & Propagation* **13**, 1811–1819.
15. **Hu W, Jia M, Dong Y, Qian X, Yang Y and He X** (2019) 3D ultra-wideband high selective bandpass FSS. In *2019 IEEE MTT-S International Wireless Symposium (IWS)* (pp. 1–3). IEEE.
16. **Zhu J, Gao W, Shi Y, Li W and Tang W** (2021) A dual-polarized band-pass frequency selective surface with stable response. *IEEE Antennas and Wireless Propagation Letters* **20**, 673–677.
17. **Hong T, Wang M, Peng K, Zhao Q and Gong S** (2020) Compact ultra-wide band frequency selective surface with high selectivity. *IEEE Transactions on Antennas and Propagation* **68**, 5724–5729.
18. **Li Y, Li L, Zhang Y and Zhao C** (2014) Design and synthesis of multilayer frequency selective surface based on antenna-filter-antenna using Minkowski fractal structures. *IEEE Transactions on Antennas and Propagation* **63**, 133–141.
19. **Xie J-M, Li B, Lyu Y-P and Zhu L** (2020) Single and dual-band high order band pass frequency selective surface based on aperture-coupled dual mode patch resonators. *IEEE Transactions on Antennas and Propagation* **69**, 2130–2141.
20. **Gurrala P, Oren S, Liu P, Song J and Dong L** (2017) Fully conformal square-patch frequency-selective surface toward wearable electromagnetic shielding. *IEEE Antennas and Wireless Propagation Letters* **16**, 2602–2605.
21. **Krushna Kanth V and Raghavan S** (2020) Design and optimization of complementary frequency selective surface using equivalent circuit model for wideband EMI shielding. *Journal of Electromagnetic Waves and Applications* **34**, 51–69.
22. **Al-Joumayly MA and Behdad N** (2010) A generalized method for synthesizing low profile, band-pass frequency selective surfaces with non-resonant constituting elements. *IEEE Transactions on Antennas and Propagation* **58**, 4033–4041.
23. **Ghosh S and Srivastava KV** (2017) An angularly stable dual-band FSS with closely spaced resonances using miniaturized unit cell. *IEEE Microwave and Wireless Components Letters* **27**, 218–220.
24. **Sivasamy R and Kanagasabai M** (2015) A novel dual-band angular independent FSS with closely spaced frequency response. *IEEE Microwave and wireless Components letters* **25**, 298–300.
25. **Coomar S, Mondal S and Sanyal R** (2022) Compact, flexible and highly selective wideband complementary FSS with high angular stability. *International Journal of Microwave and Wireless Technologies* **14**, 1298–1314.
26. **Xue JY, Gong SX, Zhang PF, Wang W and Zhang FF** (2010) A new miniaturized fractal frequency selective surface with excellent angular stability. *Progress In Electromagnetics Research Letters* **13**, 131–138.
27. **Brito DB, Araújo LM, D'Assunção AG and Maniçoba RH** (2013) A Minkowski fractal frequency selective surface with high angular stability. In *2013 SBMO/IEEE MTT-S International Microwave & Optoelectronics Conference (IMOC)* (pp. 1–4). IEEE.
28. **Khajevandi A and Oraizi H** (2021) Design of frequency selective surface based on Minkowski fractal and interdigital capacitance. *Electronics Letters* **57**, 957–960.
29. **Zhang B, Jin C, Ye X and Mittra R** (2018) Dual-band dual-polarized quasi-elliptic frequency selective surfaces. *IEEE Antennas and Wireless Propagation Letters* **18**, 298–302.
30. **Hussein MN, Zhou J, Huang Y, Kod M and Sohrab AP** (2017) Frequency selective surface structure miniaturization using interconnected array elements on orthogonal layers. *IEEE Transactions on Antennas and Propagation* **65**, 2376–2385.

Chandranath Chattopadhyaya has received his A.M.I.E.T.E degree in 2011 and M.Tech degree in electronics and communication engineering from WBUT in 2014. His main research interests are design and optimization of microstrip antenna and frequency-selective surfaces.

Srimita Coomar has obtained her B.Tech and M.Tech degree in electronics and communication engineering from MCKV Institute of Engineering under MAKAUT, WB in the years 2016 and 2018, respectively. Currently, she is associated with the Institute of Radio Physics & Electronics, the University of Calcutta as a Ph.D. (Tech.) researcher. Her main research interests are frequency-selective surfaces, microstrip antenna under the domain of RF and microwave.

https://doi.org/10.1017/S1759078723000442 Published online by Cambridge University Press

Dr. Santanu Mondal obtained his M.E in ETCE from the University of Jadavpur and Ph.D. in engineering from the University of Kalyani. He earned his B.Tech degree in ECE from Kalyani Govt. Engineering College under MAKAUT, WB. He is presently working as an assistant professor at the Institute of Radio Physics & Electronics, University of Calcutta. His area of research includes planar monopole antenna, circularly polarized microstrip antenna, frequency-selective surfaces, microwave absorber. He has contributed to various research articles in various journals and conferences of repute.

Dr. Rajarshi Sanyal has obtained his AMIETE and M.Tech degree in electronics and communication. He earned his Ph.D. in engineering from the University of Kalyani. His area of research includes microstrip antenna, microstrip filters, and frequency-selective surfaces. Presently, he is working as an assistant professor at MCKV Institute of Engineering. He has presented and published various research papers in national and international journals.

https://doi.org/10.1017/S1759078723000442 Published online by Cambridge University Press